Annals of Work Exposures and Health, 2019, 1–17
doi: 10.1093/annweh/wxz065
Original Article

Original Article

Powder Intrinsic Properties as Dustiness Predictor for an Efficient Exposure Assessment?

Neeraj Shandilya*, Eelco Kuijpers, Ilse Tuinman and Wouter Fransman

TNO, Utrechtseweg 48, 3704 HE Zeist, The Netherlands

*Author to whom correspondence should be addressed. Tel: +31-888663756; e-mail: neeraj.shandilya@tno.nl

Submitted 31 July 2018; revised 4 July 2019; editorial decision 20 July 2019; revised version accepted 25 July 2019.

Abstract

Dustiness is not an intrinsic physically defined property of a powder, but the tendency of particles to become airborne in response to mechanical and/or aerodynamic stimuli. The present study considers a set of 10 physical properties to which the powder dustiness can be attributed. Through a preliminary investigation of a standardized continuous drop test scenario, we present first set of results on the varying degrees or weights of influence of these properties on the aerosolization tendency of powder particles. The inter-particle distance is found to be the most dominant property controlling the particle aerosolization, followed by the ability of powder particles to get electrostatically charged. We observe the kinetics involved during powder aerosolization to be governed by two ratios: drag force/cohesive force and drag force/gravitational force. The converging tendencies in these initial results indicate that these physical properties can be used to model dustiness of falling powder, which can eventually be used in risk assessment tools for an efficient exposure estimation of the powders.

Keywords: aerosol; dustiness; exposure; powder; prediction

Introduction

Dustiness is defined as the propensity of a material to emit particles during handling. A measure of the dustiness can be obtained from a dustiness test (Hughes and Ogden, 1985; Hjemsted and Schneider, 1996). Dustiness is, however, not an intrinsic physical or chemically defined property of a powder. Its value depends on the characteristic properties of the powder and involved stimulus of energy. Thus, different dustiness values may be obtained by different test methods (Brouwer *et al.*, 2006; Lidén, 2006; Pensis *et al.*, 2010) for the same powder. The energy applied during dustiness tests liberates some fraction of the loosely bound primary particles and agglomerates from the bulk powder without dividing the primary particles (e.g. by grinding, cutting, or crushing) within aggregates (Lidén, 2006). Currently, two standardized test methods are generally accepted for the dustiness assessment for the handling of powders (CEN EN 15051, 2013). These are the rotating drum (Breum, 1999; Jensen *et al.*, 2009; Tsai *et al.*, 2009) and the continuous drop test (Bach and Schmidt, 2008). With certain modifications in the experimental set-up, compared with CEN 15051 (e.g. use of airborne nanoparticle sizers and counters), these two methods are also suitable for testing the dustiness of nanoscale powders (Burdett *et al.*, 2013; Tsai et al., 2009, 2011).

In a regulatory context, for the complete exposure risk assessment of powders, Organization for Economic Co-operation and Development (OECD) test guidelines necessitates the determination and reporting of dustiness data (OECD, 2016). Numerous studies have investigated the use of dustiness data to rank the potential exposure risk during handling of powders in qualitative bands, e.g. low, medium, high, and very high dustiness (Ibaseta and Biscans, 2007; Schneider and Jensen, 2008; Jensen *et al.*, 2009; Tsai *et al.*, 2009; Jensen and Levin, 2012). For risk assessment modeling tools, the conventional approach is to collectively categorize the nanoscale powders in very high dustiness category with no individual distinctions among the powders (Fransman *et al.*, 2011; Marquart *et al.*, 2008; Zalk *et al.*, 2009). However, when experimentally tested for their dustiness, some nanoscale powders have low or medium dustiness (Schneider and Jensen, 2008; Evans *et al.*, 2013). Therefore, such a conventional qualitative approach sometimes contradicts the experimental data, and the qualitative band categorization seems to be insufficient for nanomaterials.

The dustiness of a nanoscale powder and its inhalation exposure are also correlated (Heitbrink *et al.*, 1990; Breum *et al.*, 2003; Brouwer *et al.*, 2006; Evans *et al.*, 2013). For instance, Brouwer *et al.* (2006) observed the exposure concentrations to be highest for the dustiest substance and lowest for the least dusty substance. Heitbrink *et al.* (1990) found the inherent variability in the powder dustiness to be a prime factor of the variability in the exposure levels. This implies that the experimental data on dustiness is critical for an accurate estimation of the exposure risks, especially for nanoscale powders.

However, nanoscale powders are rapidly diversifying due to more and more innovation during the product design phase. In such a case, it can be useful to be able to estimate potential dustiness by using knowledge about its physical proprieties, which are intrinsic to a powder and capable of predicting its dustiness. The knowledge of such properties could be used to produce low-emissive powders (safe-by-design) and as industrial hygiene predictive parameters to ensure reduced emissions during powder handling operations (safe-by-process). Some works (O'Shaughnessy *et al.*, 2012; Evans *et al.*, 2013; Ding *et al.*, 2015; Levin *et al.*, 2015) have studied powder dustiness as a function of its intrinsic characteristic properties; however, these studies focused on one or two properties at a time.

The present study is a step toward investigating these physical properties and their influence on powder dustiness. In this study, through a series of preliminary experiments and theoretical evaluation of the aerosol kinetics, the underlying principles of the dustiness during free fall of nanoscale powders are understood and all potential dustiness influencing properties are identified. We determine whether the dustiness of a powder can be attributed to its intrinsic physical properties to estimate particle release and thus assess exposure. The experiments were conducted using a continuous drop test set-up, which mimics the dustiness during free fall or transporting powder on conveyor belts.

Material and Method

Powders

We used nine test powder samples of four different chemical compositions (TiO_2, SiO_2, $CaCO_3$, $BaSO_4$) for the study. They came from six different suppliers and were tested for their dustiness as received. To ensure the repeatability of the results, the test atmospheres were within a narrow range of temperature and humidity, i.e. 21 ± 3°C and 50 ± 5%, respectively. These conditions are within the conformity of CEN 15051. Several powder and process physical properties were characterized, and the results are provided later in the article, with more information on their commercial identities.

Characterization

Although the powders were characterized in terms of their moisture content, volume equivalent median diameter (d_{50}), dispersity (PDI), skeletal density of the agglomerate (ρ_{He}), primary particle size (d_p), work function ($\varnothing$), Hamaker constant (A), and surface composition, the process was characterized in terms of its relative humidity (RH) content and upward air velocity (U). The details of these properties and the techniques, used to characterize them, are described in Supplementary Material (available at *Annals of Work Exposures and Health* online).

Experimental set-up

In Fig. 1, we show the schematic experimental set-up used for the present study, which conforms to CEN 15051:3 and similar to other studies (Hamelmann and Schmidt, 2004; Kurkela *et al.*, 2008; Pensis *et al.*, 2010; Dahmann and Monz, 2011; Ding *et al.*, 2015).

The test chamber involves a vertical cylindrical shaped chamber (length ≈ 1200 mm and diameter = 150 mm) equipped with a HETHON 22-M-00 powder feeder at its top. As the feeder drops the powder in a controlled manner, an upward stream of air (set at controlled flow rate = 53 l/min or 0.05 m/s and controlled RH = 50%) is introduced from the bottom of the chamber, creating turbulence. The powder dosing rate is 10 g/min (except where indicated). A shear force around

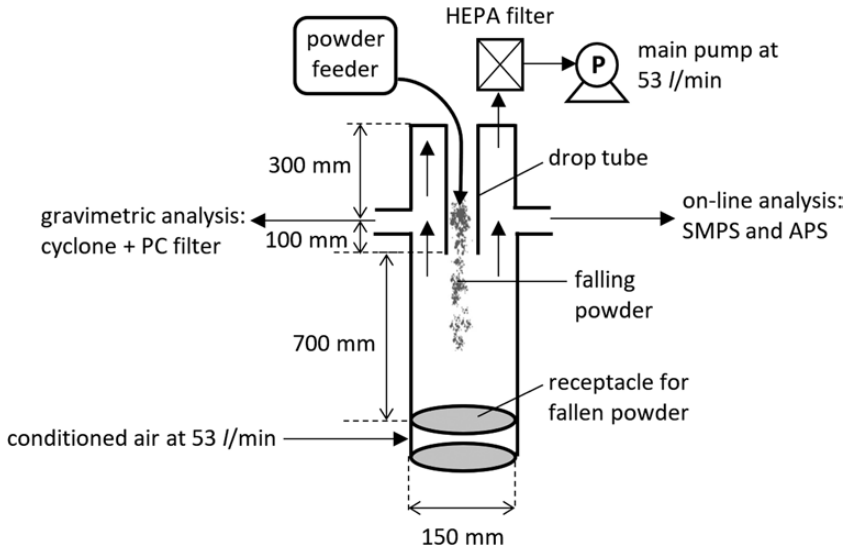

Figure 1. Schematic representation of the experimental set-up during continuous drop test of the dustiness.

the powder agglomerates is generated from the drag of the upward air flow, which leads to their aerosolization and simultaneous deagglomeration into smaller sized airborne particles. The RH level of the upstream air was also varied to study the effect of RH on the dustiness. This was achieved by varying the conditioning of air with a humidifier (Perma Pure FC125-240-5PP). Due to practical restrictions, the powder dose rate while testing the effect of RH was, however, decreased to 2.8 g/min.

Both mass- and number-based analysis of the generated airborne particles were done. For the mass-based analysis, cellulose filters were used to sample the respirable fraction of aerosol particles (i.e. particle size < 16 µm with mass median aerodynamic diameter of 4 µm or less) through a cyclone. The filters were stored in a conditioned environment (50% RH) for acclimatization prior to each test. Using a scale balance (Mettler Toledo AX205), the filters were weighed three times, both before and after the experiment to determine the averaged mass of the sampled aerosol particles. For the number-based analysis, a scanning mobility particle sizer (SMPS) and an aerodynamic particle sizer (APS) were connected to the test chamber. The SMPS and APS determine the number concentration of the airborne particles in nano- and micron-sized ranges, respectively. The details on these instruments and their operating conditions are shown in Table 1. The particle sampling points were located at 300 mm from the top of the chamber. The excess of air was pumped out of the chamber through an external induction pump (operating at 53 l/min) via a HEPA filter.

Theory

Derivation of aerosolization criteria

For continuous drop test, it is the combined action of three aerodynamic forces that act together on any sized powder agglomerate (nano or micro) during the time it passes through the vertically installed tube. These three forces are (i) gravitational force on the agglomerate; (ii) drag force from the upward air flow; and (iii) cohesive force inside the agglomerate. The gravitational force (F_g) exerted on an agglomerate, with a diameter d_a and falling with an acceleration due to gravity g, can be expressed as follows (Kulkarni *et al.*, 2011; Shandilya *et al.*, 2015):

$$F_g = (\pi \times d_a^3 \times \rho_{He} \times g)/6 \quad (1)$$

The drag force (F_d) exerted over the agglomerate by the air flow with a velocity U in the upward direction can be formulated as follows (Kulkarni *et al.*, 2011; Shandilya *et al.*, 2015):

$$F_d = \frac{\pi}{8} C_d \rho_g U^2 d_a^2 \quad (2)$$

In equation (2), $C_d = 24/Re_p$; $Re_p = (\rho_g \times V \times d_a)/\eta$; $V = \rho_{He} d_a^2 g C_c/18\eta$; $C_c = 1 + \{15.6 + 7e^{(-0.059\ p\ d_a)}\}/pd_a$, where C_d is air drag coefficient (#), Re_p is particle Reynolds number (#), ρ_g is air density (=1.2 g cm^{-3}), V is gravitational settling velocity of the agglomerate (V), η is air viscosity coefficient (=1.82 × 10^{-5} Pa.s), C_c is particle slip correction factor (#), e is electronic elementary charge (=1.6 × 10^{-19} C), p is atmospheric pressure (= 10^5 Pa). When the

Table 1. Details and operating conditions of the instruments used for the aerosol analysis during dustiness test

Instrument	Type	For	Air flow rate (l/min)	Size range	Sampling time (s)
Cellulose filter	25-mm-diameter Whatman filter	Gravimetric analysis of respirable sampled airborne particles (<4 µm)	4.2	<100 µm	NA
Cyclone	Sensidyne GK2.69	50% cut at 4 µm from the aerosol flow using centrifugal forces	4.2	≤16 µm	NA
Air pump	Sensidyne Gilian GilAir Plus	Pumping air through cyclone and filter	4.2	NA	NA
APS	Model 3321, TSI Inc.	Particle size distribution	5	0.5–20 µm	5
SMPS	DMA model 3081 + CPC model 3775, TSI Inc.	Particle size distribution	0.3 (sample flow rate) 3 (sheath flow rate)	14–673 nm	120

NA, not applicable.

agglomerate constituting primary particles are in contact and some water/moisture is present in between them, capillary bridges are formed in the gap between the particles and they induce a cohesion force. Alternatively, capillary condensation occurs when humidity of the air condenses moisture into the gap between particles and the liquid forms a meniscus there. In either case, the meniscus induces the cohesion force due to (i) the pressure difference between liquid and gaseous phase and (ii) the surface tension on the liquid–gas interface. The capillary condensation is important, especially for nanoscale particles for which the capillary pressure inside the meniscus is far greater (Dörmann and Schmid, 2015). If Δp is the pressure difference between inside and outside of the water meniscus existing between two particles, then $\Delta p = \gamma / r_K$, where γ is surface tension (N m^{-1}) and r_K is Kelvin radius (m) ($r_K = (\gamma V_M)/\mathrm{RT.ln(RH)}$), V_M is molar volume of water at room temperature (m^3/mol), R is gas constant (= 8.314 kg m^2 s^{-2} K^{-1} mol^{-1}) and T is ambient or room temperature (=298 K). For an average value of the inter-particle distance r, surface tension (γ) and water contact angle with the particle's surface α, the combined capillary force (Dörmann and Schmid, 2015):

$$F_c = (\Delta p) \quad \pi r^2 + \gamma(2\pi r)\cos\alpha \tag{3}$$

When two particles rub against each other, an electrostatic charge is transferred from one to the other (Yao *et al.*, 2004). The charge transfer can be explained in terms of electron transfer arising from the work function value of the particle material (Matsusaka and Masuda, 2003). Assuming that electron transfer takes place by tunneling so that thermodynamic equilibrium prevails, the contact potential difference is, $V' = -\varnothing/e$ (Harper, 1951). The amount of the transferred charge is, $q = CV$. The capacitance of a particle with a primary particle size d_p is equal to $C = 2\pi\varepsilon_0 d_p$, ε_0 is the permittivity of free space (=8.854 × 10^{-12} F/m). According to the Coulomb's law, the electrostatic force between two primary particles inside an agglomerate is equal to:

$$F_e = k\frac{q_1 . q_2}{r^2} \tag{4}$$

Here k is Coulomb's constant (= 8.99 × 10^9 N m^2 C^{-2}). The average value of the inter-particle distance, i.e. r is the indicator of the powder compactness. In other words, the more the powder is compacted, the lower is its value of r. With the increase in powder compaction, its bulk density also increases. Therefore, r can also be considered as an indicator of the powder bulk density. Depending on the size of a primary particle and its distance from other primary particles, it ubiquitously interacts with them through van der Waals forces (F_{vdw}) of attraction (Ding *et al.*, 2015).

$$F_{vdw} = \frac{Ad_{p1}d_{p2}}{12r^2\left(d_{p1} + \quad d_{p2}\right)}. \tag{5}$$

The Hamaker constant, A, is a material constant that depends on the particle material properties and the intervening media (air in the present case). Hence, the total cohesive force, F_{coh}, acting inside an agglomerate can be written as the sum of F_c, F_e, and $F_{vdw,}$ i.e.

$$F_{\text{coh}} = \left\{(\Delta p) \quad \pi r^2 + \gamma(2\pi r)\cos\alpha\right\} + \left|k\frac{q_1.q_2}{r^2}\right| + \frac{Ad_{p1}d_{p2}}{12r^2(d_{p1} + \quad d_{p2})} \tag{6}$$

From equations (1), (2), and (6), for an agglomerate to get/remain airborne, the drag force acting on it should be greater than its gravitational force, i.e.

$$F_{\text{d}} > F_{\text{g}} \tag{7}$$

If not, the drag force should be sufficient for the deagglomeration, i.e.

$$F_{\text{d}} > F_{\text{coh}} \tag{8}$$

The agglomerate breaks into smaller sizes with reduced F_{coh}. The two ratios, F_d/F_g and F_d/F_{coh}, measure the tendency or likeliness of an agglomerate to aerosolize (Higashitani *et al.*, 2001). An increase in their values indicates a significantly higher aerosolization tendency.

Sensitivity analysis

As shown earlier, the aerosolization tendency of a powder to de-agglomerate is considered to be a function of several properties related to the powder and process. A certain change in the values of these variable properties may impart different changes in the aerosolization tendency, depending on how influential is the property compared with the agglomerate aerosolization. To investigate the influences, a sensitivity analysis of the percentage change in the values of F_d/F_g and F_d/F_{coh} (i.e. aerosolization tendency) was carried out using one-at-a-time (OAT) method (Delgarm *et al.*, 2018; Hamby, 1994). Three sets of arbitrarily chosen base values (typical average values) were assigned one by one to the variables and values of F_d/F_g and F_d/F_{coh} were deduced from equations (7) and (8), which correspond to these base values. The base values were then increased and decreased by 25% to compute the percentage change in F_d/F_g and F_d/F_{coh} values. While doing this, one property was varied at a time and the others were kept fixed.

Results

Characterization

In Table 2, we show the results from different characterization tests carried out on nine test powders. The values of ∅ and A were taken directly from the literature.

Aerosolization tendency

The Fig. 2a shows the variation of F_d/F_g [equation (7)] with increasing value of the agglomerate size and a constant skeletal density ($\rho_{He} = 1.2$ g/cm^3) for two different values of U. With an increase in the agglomerate size, its tendency to aerosolize decreases monotonously. The agglomerate size of ~20 μm is the maximum limiting size for U = 0.05 m/s. The limiting size increases to ~50 μm when U = 0.2 m/s. For an agglomerate size of 1 μm, the F_d/F_{coh} is plotted against r in Fig. 2b for two different values of U. The tendency to aerosolize first increases with an increase in r and then decreases once $r > 10^{-3}$ μm. The aerosolization tendency for U = 0.05 m/s is limited to a specific range of r values, i.e. $r \in [5 \times 10^{-4}$ μm, 5×10^{-3} μm]. With U = 0.2 m/s, the aerosolization tendency does not only increase, but the range of the r values also increases, i.e. $r \in [2.5 \times 10^{-4}$ μm, 1.2×10^{-2} μm]. Clearly, the aerosolization tendency is sensitive to the variation in the values of d_a, r, and U.

In Fig. 3a–c, we further enquire about the effect of r on the cohesive forces between different sized particles with same PDI (= 0.6). In Fig. 3a, we consider it for two particle size modes of 2 and 5 nm, respectively. When $r \leq 10^{-3}$ μm, both F_e and F_{vdw} are decreasing whereas F_c is increasing and F_e is the most dominating cohesive force. Consequently, the total cohesive force, F_{coh}, is almost equal to it and decreases with an increase in r. When $r > 10^{-3}$ μm, F_c starts to dominate the other two cohesive forces and approximates F_{coh}. Butt and Kappl (2010) attributed this observation to an easy uptake of the water at higher values of r. Hence, F_{coh} now starts increasing. F_{coh} holds a minimum value, i.e. $(F_{coh})_{min} = 4.5 \times 10^{-9}$ N at $r = 10^{-3}$ μm for 2 and 5 nm particle mode sizes. It is the change in the type of the dominant cohesive force that makes F_{coh} to first decrease and then increase. This also leads to the similar variations of F_d/F_{coh} in Fig. 3b. The $(F_{coh})_{min} = 10^{-6}$ N at $r \approx 0.02$ μm when the particle size modes are increased to 1.25 and 0.5 μm (Fig. 3b). $(F_{coh})_{min}$ further increases to 10^{-5} N at $r \approx 0.09$ μm when the particle size modes are increased to 8 and 20 μm (Fig. 3c). Therefore, an increase in the primary particle size mode leads to the increase in both total cohesive energy and inter-particle distance needed to attain minimum cohesive energy.

A sensitivity analysis is shown in Fig. 4 to theoretically determine the physical properties that influence the aerosolization tendency. In Table 3, three sets of arbitrarily chosen base values of each variable are shown. The variable base values in each set are changed by ±25% to observe its effect on the % change in the aerosolization tendency of an agglomerate. The results produced from three sets of variable base values are then averaged and shown as rectangular bars with

Table 2. Characterization of the test powders

#	Powder (producer/ supplier)	Surface composition	Moisture content (%)	d_{50} (µm)	ρ_{He} (g/ cm^3)	PDI (#)	d_p (nm)	Ø[a] (eV)	A[b] (× 10^{-20} J)	Bulk density (g/cm^3)	Respirable mass-based DI (mg/kg)	Particle mode size (nm)/peak number concentration (#/ cm^3)
1	AT1 TiO_2; anatase (Cristal)	Not tested	14.2	0.52	3.9	2.7	43	5.7	15.3	1.2	0.8	Not tested
2	P25 TiO_2 (Evonik)	Not tested	0.3	0.8	3.6	2.1	48			1.31	9	322/3945
3	PC105 TiO_2; anatase (Cristal)	Not tested	17	4.2	2.3	1.25	50			0.88	2.2	Not tested
4	NM103 TiO_2; rutile (JRC-IHCP)	Dimethoxy dimethylsilane (hydrophobic)[c]	Not tested	1.6	Not tested	2.23	66			Not tested	Not tested	289/11 148
5	NM104 TiO_2; rutile (JRC-IHCP)	Tetramethyl silicate (hydrophilic)[c]	10.4	1.4	3.2	2.22	62			0.78	22	487/38
6	4850MR SiO_2 (Nanoamor)	Not tested	4.2	9.6	1.9	0.67	22	1.78	6.5	0.14	150	445/6100
7	1951RH $CaCO_3$ (SSNano)	Not tested	7.2	2.4	3.4	2.5	90	2.87	10.1	0.73	9	Not tested
8	1955RH $CaCO_3$ (SSNano)	Not tested	0.7	7.6	2.6	1.8	50			0.54	60	Not tested
9	U107 $BaSO_4$ (Solvay)	Not tested	1.4	3	2.1	1.3	40	2.52	Not available	0.32	100	Not tested

[a]Lide (2004).
[b]Bergström (1997).
[c]Rasmussen *et al.* (2014).

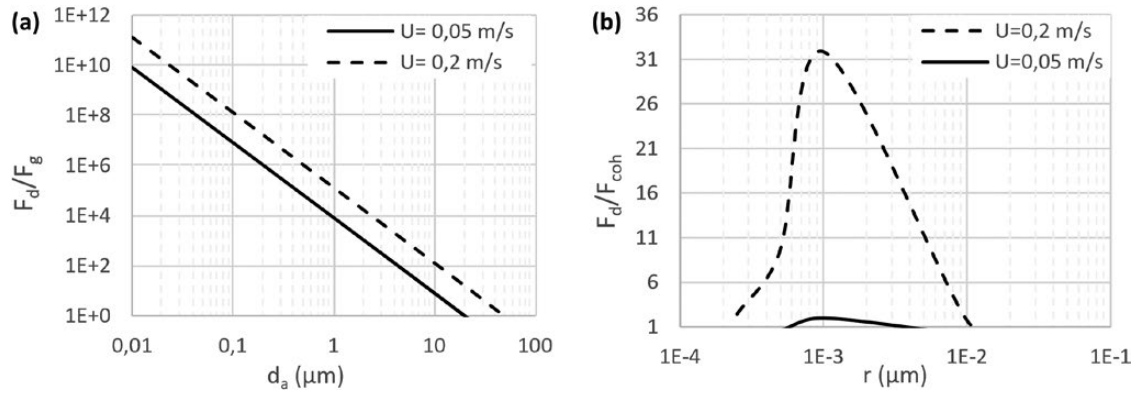

Figure 2. (a) F_d/F_g as a function of agglomerate size and (b) F_d/F_{coh} as a function of average inter-particles distance when the powder with same skeletal density (= 1.2 g/cm^3) is subjected to two different upward airflow velocities.

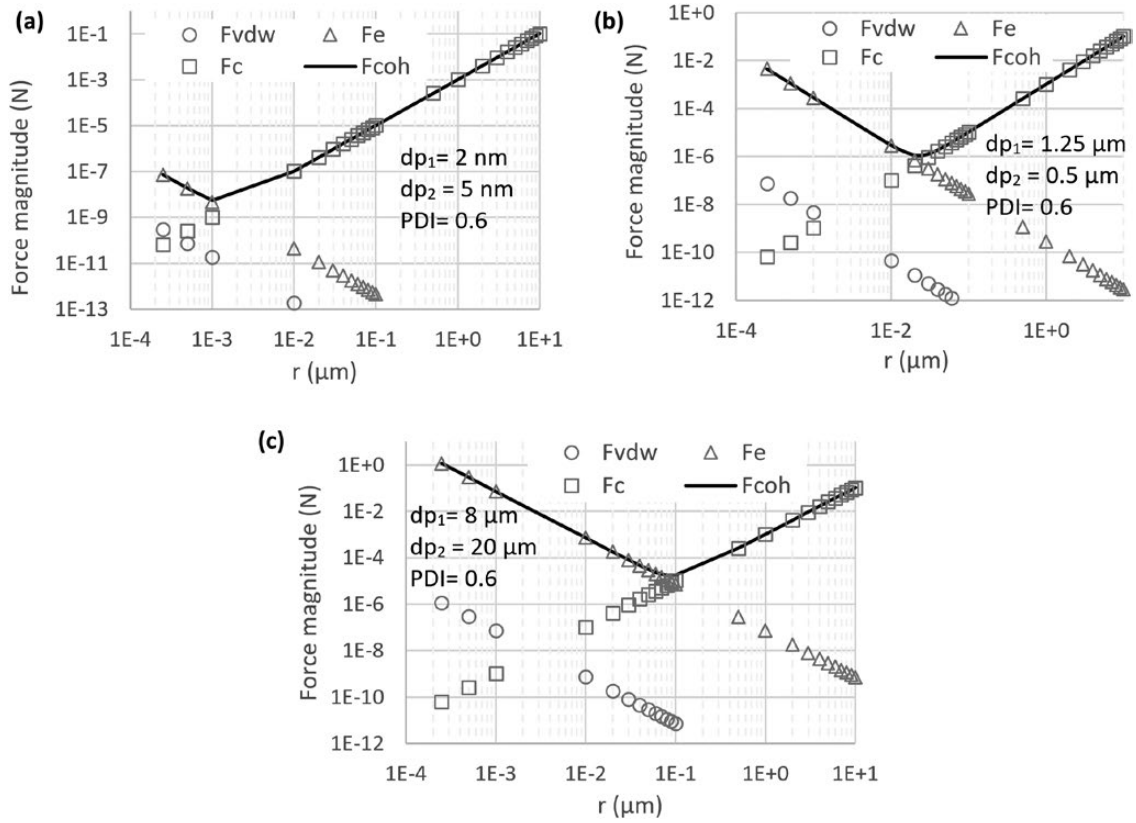

Figure 3. Influence of the average inter-particles distance on the cohesive forces when the particle size modes are equal to (a) 2 and 5 nm, (b) 1.25 and 0.5 µm, (c) 8 and 20 µm.

errors bars corresponding to the reproducibility over three sets in Fig. 4.

A 25% increase in the base value of *r* results in an almost 78% increase in the average change in the aerosolization tendency of an agglomerate. A 25% decrease in *r*, however, produces ~44% decrease in the average value. This is a non-linear and largest % change in the aerosolization tendency (= 78-(-44) = 122%) that we could observe for any variable. For *U*, the aerosolization tendency increases non-linearly by a mean

value of 67% with a 25% increase in the base value and decreases by a mean value of 34% with a 25% decrease. Therefore, the % change = 67-(-34)= 101%. The other variables in decreasing order of their influence (with respective % changes in the aerosolization tendency) are as follows: ∅ (80%) > ρ_{He} (60%) > d_p (40%) > PDI (35%) > RH (25%) > d_{50} (21%) > α (11%) > A (2%). Clearly, the aerosolization tendency of an agglomerate is most sensitive to r and the sensitivity decreases in the aforementioned order.

Experiments

Using the gravimetric analysis of the sampling filters in the continuous drop configuration of the dustiness test, we experimentally determined the mass-based respirable dustiness indices (DI in mg/kg) (n = 3). The average DI values are shown in Table 2 and plotted in Fig. 5 as color-coded data points showing the corresponding powder samples. In Fig. 5a, the influence of powder bulk density (as per CEN 15051) is shown where an increase in the bulk density leads to a decrease in DI (R^2 = 0.98 of the fitted curve), except for the last data point (corresponding to powder #2) for which DI slightly increases. It can be the effect of lower moisture content of powder #2 (moisture content = 0.3%) than powder #9 (moisture content = 1.4%). A negative correlation of DI holds true with ∅ (R^2 = 0.88 of the fitted curve), as shown in Fig. 5b. However, multiple DI values were observed for a single value of ∅ in some cases. Since the powders #7 and 8 ($CaCO_3$) have the same elemental composition, they have same values of ∅. Similarly, TiO_2 powders #1, 2, 3, and 5 have same value of ∅. The DI monotonously decreases with increasing ρ_{He} of the powder samples in Fig. 5c, i.e. a negative correlation (R^2 = 0.71 of the fitted curve). In accordance with Fig. 4, the same observations can be made for d_p and PDI where DI decreases with increase in their values (Fig. 5d,e; R^2 = 0.69 and 0.66 of the fitted curves respectively). On the contrary, with d_{50}, we observe that DI has a positive correlation (R^2 = 0.61 of the fitted curve) in Fig. 5g. This result also agrees with Fig. 4. The dependence of DI on moisture content in Fig. 5f is rather complicated where DI first increases (until moisture content = 4%) and then decreases with increasing moisture content. Similar to ∅, A has a negative correlation with DI, as shown in Fig. 5h (R^2 = 0.58 of the fitted curve). The R^2 values in Fig. 5a–h appear to follow the same decreasing order as their influence on the aerosolization tendency in Fig. 4.

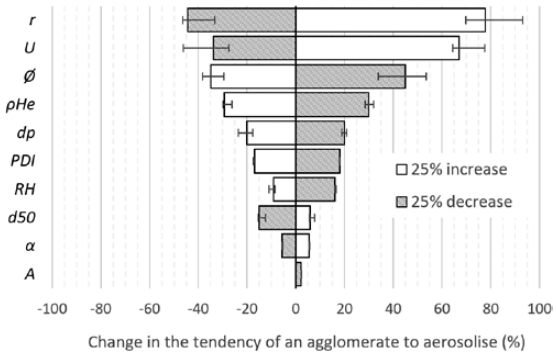

Figure 4. Sensitivity analysis of the aerosolization tendency of a powder agglomerate; errors bars correspond to the reproducibility over three sets of base values.

In Fig. 6, we illustrate the effect of powder charging (tribologically charged by shaking them inside their plastic packaging prior to the dustiness test) on the number concentration of airborne particles. The number concentrations in Fig. 6a,b correspond to SiO_2 powder (#6 in Table 2) and the ones in Fig. 6c,d correspond to TiO_2 powder (#2 in Table 2). These number concentrations are normalized values obtained after dividing them by the corresponding feed rate of the powder. We see a clear decrease in the number concentration of airborne particles when the powder is charged, whether it is nanometric size range (measured by SMPS; Fig. 6a,c) or micrometric size range (measured by APS; Fig. 6b,d). Such clear effect of powder charging, however, cannot be observed on the size mode of these particles in any case.

The effects of U, α, and RH on dustiness were studied for hydrophobic (NM103; α > 90°) and hydrophilic (NM104; α < 90°) TiO_2 powders (see Table 2). The results are shown in Fig. 7. Similar to Ding *et al.* (2015), we observe that higher U generates smaller mode sizes (Fig. 7a). When $U \leq 1$ m/s, the particle sizes decrease rapidly but this tendency slows down beyond this limit. We observe similar patterns for both NM103 and NM104

Table 3. Base values of the variable properties considered for the sensitivity analysis

Variable	r (nm)	U (m/s)	∅ (eV)	ρ_{He} (g/cm^3)	d_p (μm)	PDI	RH (%)	d_{50} (μm)	α (rad)	A (×10^{-20} J)
Base values set 1	0.5	0.1	4	3	0.5	0.5	50	1	π/2	15.3
Base values set 2	1	0.2	3	4	0.01	0.01	20	2	π/3	4.05
Base values set 3	2	0.05	3.6	2	2	2	60	0.5	2π/3	24.6

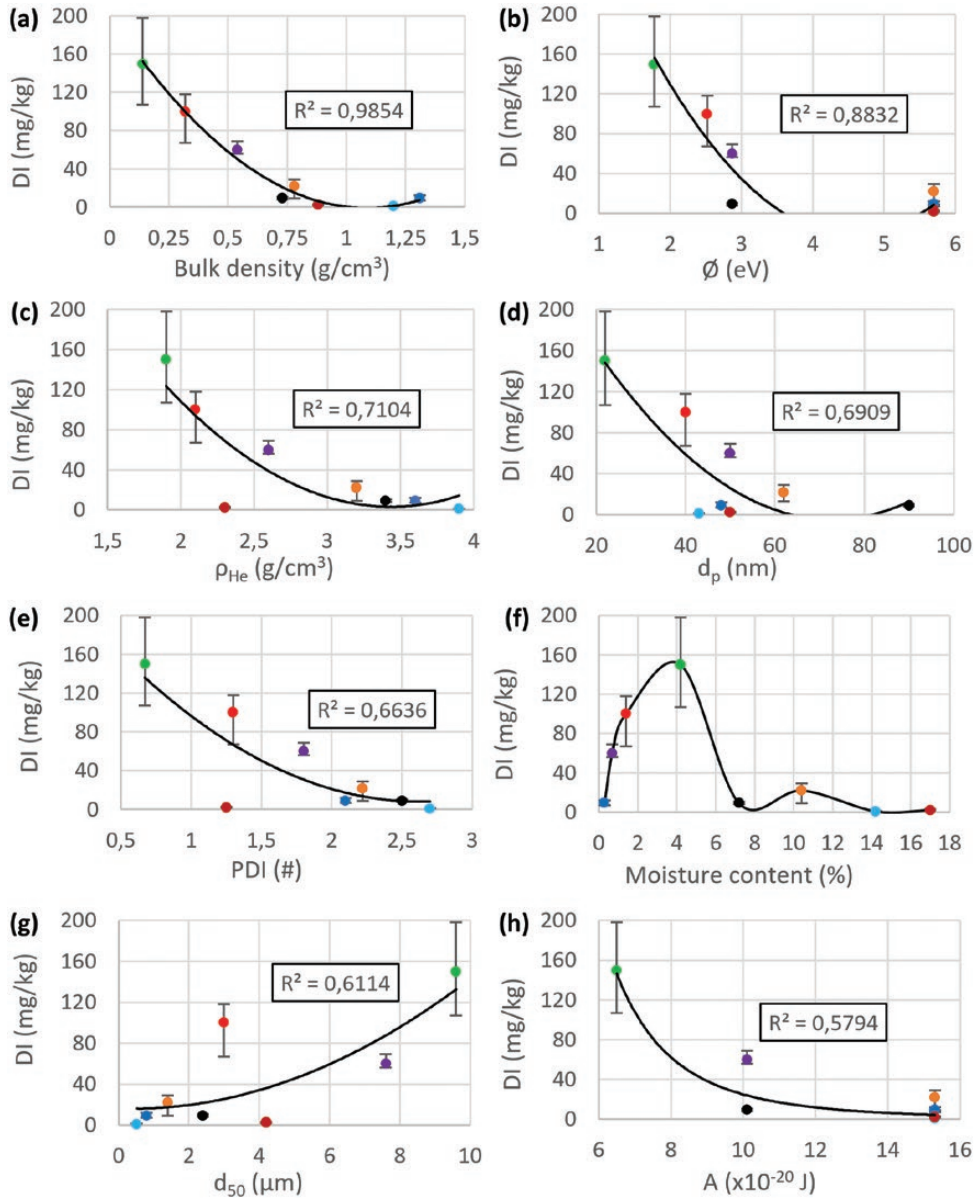

Figure 5. Experimentally measured dustiness index as a function of (a) bulk density; (b) Ø; (c) ρ_{He}; (d) d_p; (e) PDI; (f) moisture content of powder; (g) d_{50}; (h) *A*. The data points corresponding to the powders #1–9 (except #4 for which DI was not determined) are color coded: #1: light blue; #2: blue; #3: dark red; #5: orange; #6: green; #7: black; #8: purple; #9: red. The coefficient of correlation (R^2) of the fitted curve with dustiness index for each property is shown in each case (except for moisture content).

particles. Overall, the hydrophobicity of the particles leads to a decrease in the mode size of aerosolized particles. When analyzed for the number concentration at U = 0.5 m/s, similar to Burdett *et al.* (2013), we observe higher concentration for NM103 (peak concentration= ~1.1 × 10^4 #/cm³) than NM104 (peak concentration= ~38 #/cm³) in the size range of <500 nm, determined by SMPS (Fig. 7b).

For the size range > 500 nm, determined by APS (Fig. 7c), NM104 has higher concentration (peak concentration= ~32 #/cm³) than NM103 (peak concentration= ~8 #/cm³). Therefore, the airborne particles, generated by hydrophobic powder, dominate in nano and submicrometric size range (i.e. smaller sized particles), whereas the hydrophilic powder tends to generate more microparticles (i.e. bigger sized particles).

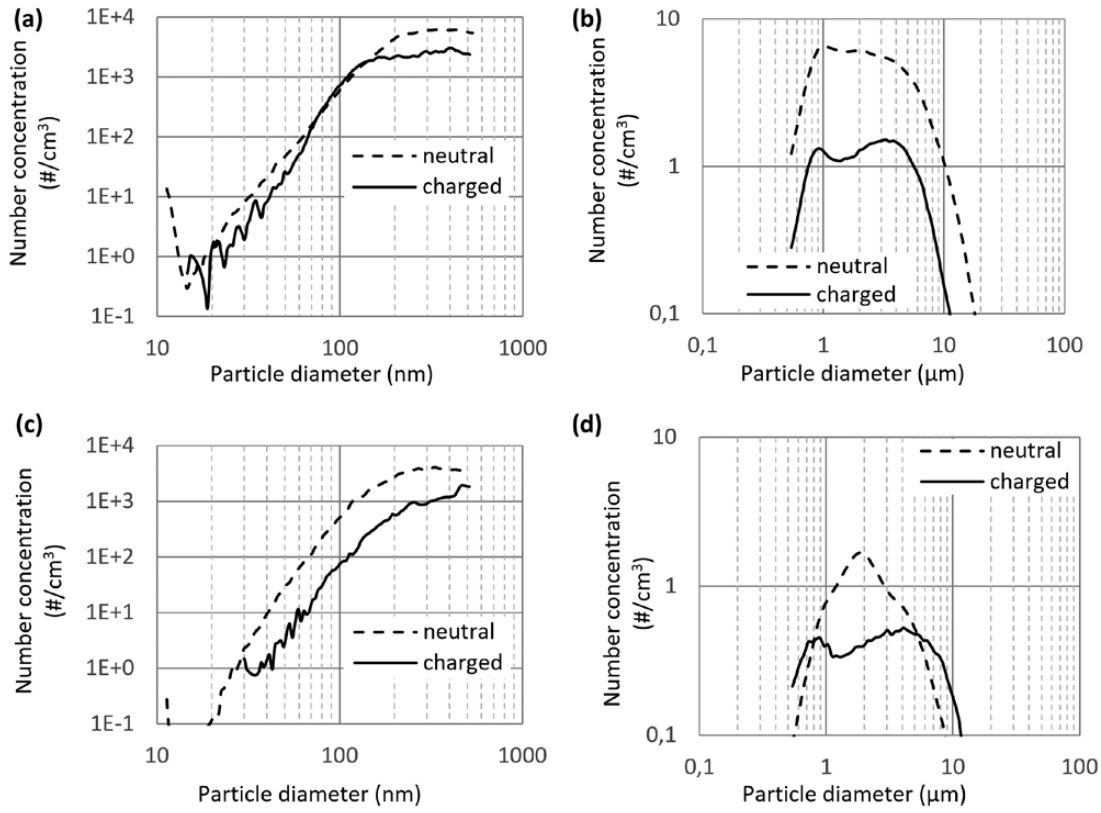

Figure 6. Difference in the particle size distributions of the airborne particles when the SiO_2 powder is charged or neutral as given by (a) SMPS and (b) APS; similar size distributions for TiO_2 powder as given by (c) SMPS and (d) APS.

The same tendency can be observed when the effect of RH was investigated. An increase in RH leads to a decrease in the mass concentration of airborne particles. For the particles size range < 0.5 µm (measured using SMPS), NM103 tends to generate higher concentration than NM104 (Fig. 7d). The rate of change of the concentration is higher though for NM104 (slope of the fitted linear curve = −0.0021) than NM103 (slope of the fitted linear curve = −0.0012). For the particle size range from 0.5 to 4 µm (Fig. 7e), NM104 generates higher concentration, similar to Fig. 7c. Again, the rate of change of the mass concentration is higher for NM104 (slope of the fitted linear curve = −2.257) than NM103 (slope of the fitted linear curve = −0.528). This clearly shows that the effect of changing RH is more pronounced on the hydrophilic powder than the hydrophobic one.

Discussion

The objective of the present study was to (i) understand the underlying principles involved in the aerosolization of powder particles during continuous drop test and (ii) determine whether the dustiness of a powder can be attributed to some intrinsic physical properties to estimate particle release. Given the fundamental importance of accurate characterization of nanomaterials for risk assessment, these intrinsic properties have been obtained for a limited number of powders and within the scope of this study. A preliminary assessment shows that 10 physical properties (8 powder related and 2 process related) can have a critical influence on the aerosol emission tendency of a powder during its handling activities. Due to their varying weights of influence on DI, each of these powder properties did not show a good correlation with DI (R^2 of the fitted curves varied between 0.58 and 0.98). Nevertheless, the level of correlation was observed to follow the same order of influence as in the sensitivity analysis. The simulation was carried out by using the continuous drop test. Therefore, the results should be interpreted in the context of only continuous drop configuration. Once fully developed, the same approach can also be applied to the standard methods of rotating drum, small rotating drum, and vortex shaker.

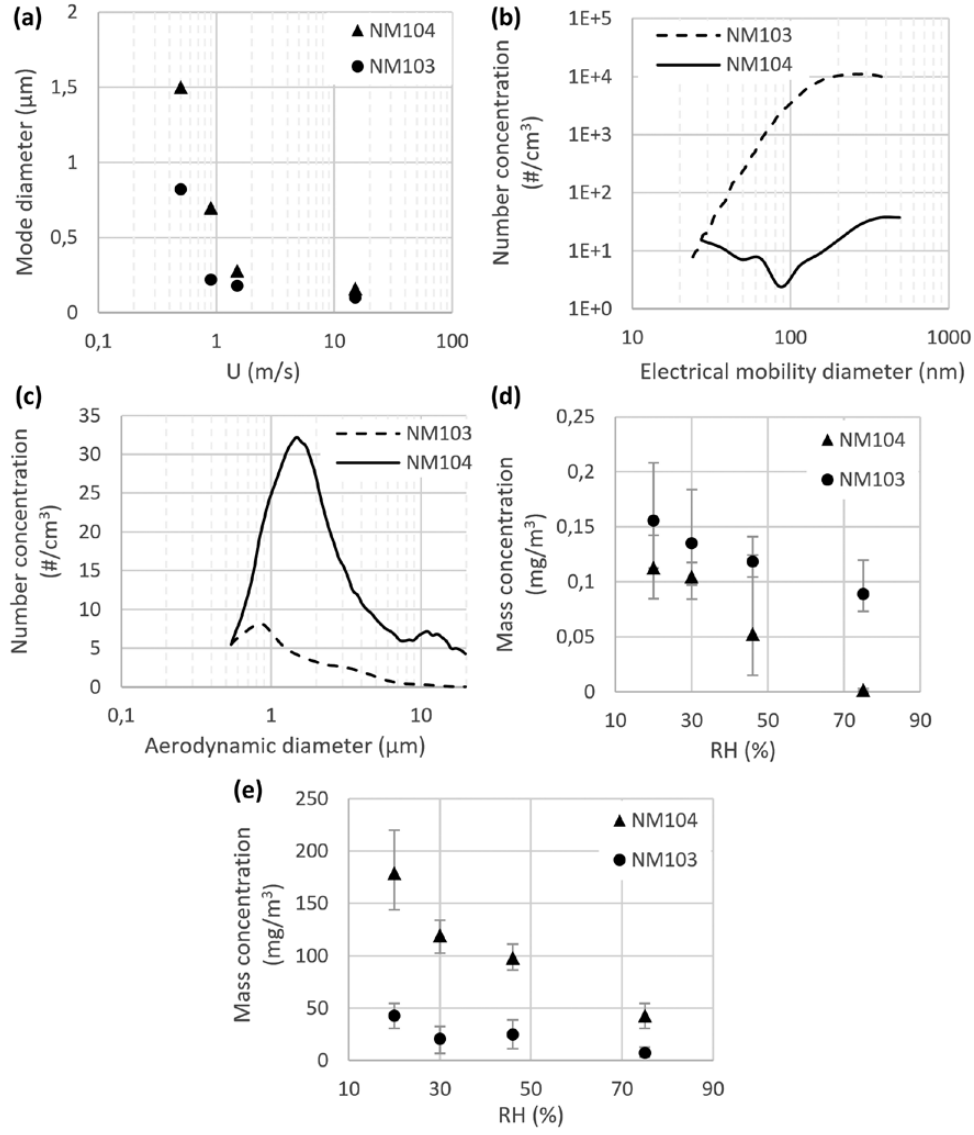

Figure 7. Influence of (a) *U* on mode diameter of airborne particles for both hydrophobic (NM103) and hydrophilic (NM104) TiO_2 powder particles; influence of particle hydrophobicity or hydrophilicity on the size distribution of the generated airborne particles given by (b) SMPS and (c) APS; influence of RH on the mass concentration of airborne particles with size (d) < 0.5 µm given by SMPS and (e) between 0.5 and 4 µm given by APS.

Physical properties

In our study, we found that the most influential physical property of the powder is the average inter-particle distance between its constituent particles, i.e. *r* (van Ommen *et al.*, 2012). This variable physically signifies the compaction state or the bulk density of the powder. When the interfacial potential is minimal between two particles, an equilibrium stage is reached and *r* holds a steady value (Cheng *et al.*, 2002). Therefore, *r* can be viewed as the powder particle van der Waals radius (Batsanov, 2001). If the regression between *r* and the bulk density be assumed to be approximated by a distribution function (linear, polynomial, log-normal, exponential, etc.), then a certain % change in *r* will impart certain % change to the bulk density. While studying the effect of the bulk density on the dustiness of a Bentonite powder sample, Jensen *et al.* (2009) found that even a low-pressure of 3.5 N increased the bulk density of Bentonite powder

in a logarithmic manner and reduced the dustiness index by ~20%. In other words, they concluded that by decreasing r (via an increase in bulk density or physical loading), DI decreases which reiterates the observation from Fig. 4. When r is combined with RH, it results in the storage conditions of the powder. Levin *et al.* (2015) studied the effect of such storage conditions on different material type powder samples by subjecting them to constant load of 2.7 kg and different RH levels (30, 50, and 70%) over a week. They observed powder material-dependent decrease in DI, with an exception of RH = 70%, for which the powder compaction resulted in the increase of DI. They attributed this exception to high compaction of the material which limited the uptake of water—an observation in agreement with Fig. 3.

The second most influential property is process related, i.e. U. It is the primary measure of the drag force or shear energy to which powder particles are subjected when falling down from the feeder. When U increases, the test protocol provides more energy and, thus, the fraction of aerosol generated increases. The main reason is the high likeliness of powder deagglomeration. The relatively smaller sized airborne agglomerates (Fig. 7a) result in a shift of particle size mode to the smaller size range. In an agglomerate, the cohesion energy is imparted by the cohesive forces present inside the agglomerate. For the same process/application conditions, high cohesion energy leads to the powder dustiness diminution (Bouillard *et al.*, 2014). Therefore, from this perspective, to prevent the occupational exposure risks of dustiness during powder handling, the cohesive force should be maximized. However, high cohesive force causes hindrance to the powder flowability—a property that dictates the quality and content uniformity of the end products in several pharmaceutical processes. To avoid any segregation problem, the powder processing industries heavily rely on the good flowability of the powder which can only be imparted with low cohesive forces (Prescot and Barnum, 2000; Seipenbusch *et al.*, 2010; van Ommen *et al.*, 2012). Hence, the cohesive forces within the powder agglomerates should be optimized for maximum cohesive forces possible without compromising with the powder flowability.

The effect of Ø on the aerosolization tendency of powder particles is the third most influencing property. It is the primary factor that accounts for the ability of any powder to be electrostatically charged. Higher value of Ø indicates easiness toward gaining a charge. For no or very low moisture content, the electrostatic force is the most dominating one acting within the powder particles. With an increase in the moisture content, Mukherjee *et al.* (2016) demonstrated the electrostatic force of attraction to get nullified due to the decrease in the element work function. We believe that it leads to the increase in DI. This continues until the moisture content <4% (in the present case). Beyond this limit, the moisture within the powder is now enough to generate strong capillary forces of attraction within the powder particles. This then leads to the decrease in DI. In our experimental results, we have obtained multiple DI for same Ø in, for instance, powder samples #1, 2, 3, and 5 (Fig. 5b). One should remember that the values of Ø were not measured but directly taken from the literature (Lide, 2004) in this study. The difference in their DI values can thus be attributed to the differences in their respective moisture contents. A clear dependence of DI on Ø can only be derived in the case of powders with similar (preferably same) moisture content but different elemental compositions.

Apart from the powder moisture content, RH can also greatly affect particle charging tendency. In an experimental study, Greason (2000) measured the charge on a metal sphere with a Faraday cage with varying RH. At a given temperature, the charge monotonously decreased with increasing RH. The increased leakage caused by a decrease in the electric resistance on the surface resulted in this decrease in charge. Nomura *et al.* (2003) found that the charge decreased even more rapidly when the charged particles are kept at higher RH. An increase in RH can also lead to an increase in the net moisture content of the powder. This results in a direct decrease in the powder dustiness. The effect is observed to be more pronounced for hydrophilic powder than hydrophobic one (Fig. 7d,e). One probable reason can be the higher affinity of hydrophilic powder toward water vapors in highly humid air which rapidly increases their net moisture content, thus forming faster and stronger capillary bridges between the powder particles and increasing F_c.

Another powder property, PDI, is negatively correlated with DI. Brouwers (2006) and Dexter and Tanner (1972) showed that with increasing DI, the particles pack to higher-volume fractions because the smaller particles pack more efficiently by either layering against larger particles or fitting into the voids created between neighboring large particles. It implies r to hold a low value and thus lower DI. Andreasen *et al.* (1939) also confirmed that PDI inhibits DI of a powder by adding fine particles (<10 μm) to relatively coarse ones (but dusty), and observing reduction in the dust generating capacity of the final powder with greater PDI.

The least influencing powder property was found to be A. It is a material constant that depends on the particle material properties and the intervening media (air

in the present case). Thus, in principle, the powder samples with same composition and intervening medium should have same DI. However, that is not the case in Fig. 5h where powder samples #1, 2, 3, and 5 have same *A*, but different DI. An easy domination or obscureness of the influence of *A* on DI by other powder properties can lead to such discrepancy in the experimental result.

Dustiness and personal exposure

As per the current practices, for the exposure risk assessment (RA) of a powder, its dustiness is tested and is provided as input in the RA tools. However, quantitative dustiness information is often lacking and hence RA tools use qualitative categorization system to estimate the powder's emission potential or assign conservative exposure values to nanoscale powders. The generic exposure RA tools such as Stoffenmanager (Marquart *et al.*, 2008), Control Banding Nanotool (Zalk *et al.*, 2009), and Advanced REACH Tool (ART) (Fransman *et al.*, 2011) are using qualitative dustiness classes as input for substance emission potential of powder in general. For example, ART considers the dustiness to be influenced by the moisture content with an assumption that higher the moisture content, smaller is the propensity to become airborne. However, in Fig. 5, we have seen DI to first increase and then decrease with increasing moisture content. Therefore, such qualitative assignment of dustiness category of a powder appears to be conservative and insufficient to estimate the real personal exposure.

Although preliminary, the first set of dustiness results of this study converge to particular dustiness influencing tendencies of powder physical properties and inter-properties interactions. In the future, we intend to model dustiness, so that it can be estimated on the basis of these identified properties. This can be pursued through a detailed study with a full factorial experimental design of ten parameters, higher number of tested powders and comprehensively characterized physical properties. The powders made of mixed particle sizes (nano and sub-micro) can also be included to observe if these tendencies and interactions hold true in their cases too. Moreover, the study can assess how differently inhalable DI (aerosol particle size > 4 µm) correlate with the powder physical properties when compared with the respirable DI. The estimated dustiness can then be compared with the experimentally measured values for the purpose of performance and reliability evaluation of the model. If found reliable, the dustiness model could then be included in the existing exposure RA tools which will ensure an efficient exposure estimation of the powders by these tools. The dustiness model can also be tested to see whether one model fits all standard dustiness test set-ups such as rotating drum, short rotating drum, and vortex shaker. The required user-specific information on process-related properties of these test set-ups can be modified accordingly.

For a user, a powder product is not (always) accompanied by the information on these nine influential properties. This makes it difficult for a user to have their knowledge without doing the characterization tests (as done in the present study). Therefore, it can be argued that determining the values of these properties can be an additional task and time consuming. However, as shown in Table 4, these nine influential properties (except ∅ and *A*) are generally the pre-requisites for reliable functioning of frequently used advanced RA tools such as NanoSafer, GuideNano, etc. The OECD Working Party on Manufactured Nanomaterials (WPMN) also necessitates these properties in the list of the material characterization endpoints for complete hazard profiles of various representative manufactured nanomaterials (Rasmussen *et al.*, 2014). Therefore, the performance of required characterization tests to identify these nine properties is quintessential for complete exposure and hazard assessment study of nanomaterials. The aforementioned future dustiness model can then be used for dustiness estimation and not perform the dustiness test as an additional task.

Moreover, with rapidly diversifying nanoscale powders due to more and more innovation during the product design phase, the knowledge of these eight powder properties would lead to the safe innovation during the industrial production and processing of powders, i.e. safe-by-design approach. As per the Stage Gate® model (Cooper, 2008), this knowledge can be gained via various characterization techniques during the experimental development phase. It would ensure that the dustiness is reduced to its minimum level possible during powder testing and validation phase, i.e. prior to the market launch and full powder production phase.

Sensitivity analysis

In the present study, we see interactions among different properties, e.g. the dependence of Ø on RH, dependence of RH on *r* etc. The OAT method used in the present study, however, cannot account for such interactions among different variables, as all variables are considered equally likely in this method. Numerous theoretical combinations of variables prohibit an attempt to systematically account for all potential interactions. Also, most of such interactions are still unknown as per our knowledge. Therefore, the data presented in Fig. 4 may involve uncertainties, which are not presently taken into account.

Theoretical evaluation

By balancing the forces acting in and around a powder agglomerate, we developed two criteria [equations (7) and (8)], which are considered to be essential for powder agglomerate to aerosolize. Instead of predicting DI value for any powder, i.e. the aerosolized mass of the powder, we have developed these two criteria that evaluate the likeliness toward aerosolization. We undertook the following assumptions while developing these criteria: (i) once dispersed, the powder particles do not reagglomerate when collided; (ii) radius of the water meniscus cross-section between two powder particles can be approximated as the distance between them; and (iii) the medium around an agglomerate/particle while falling down is air at atmospheric pressure and room temperature. Under given process conditions, higher the values of F_d/F_g and F_d/F_{coh} for a powder, higher is its tendency to emit the airborne particles. A reduction in the value of these two ratios will result directly in the reduction of DI of any powder. The best way to reduce these ratios is to control the most influencing properties (from Fig. 4).

This approach can also be further developed toward the quantification of the aerosolized mass of the powder. For this, instead of considering a whole agglomerate, we may consider the average number of individual primary particles contained within an agglomerate, i.e. Average Agglomeration Number (AAN). Equations (1) and (6) can thus be transformed as follows:

$$F_g = \sum_{i=1}^{AAN} \left[(\pi \times d_{pi}^3 \times \rho_p)/6 \right] \tag{9}$$

$$F_{coh} = \sum_{i=1}^{AAN} \sum_{j=1}^{AAN} \left[\left\{ \frac{A d_{pi} d_{pj}}{12 r_{ij}^2 (d_{pi} + d_{pj})} \right\} + \left\{ (v) \quad \pi r_{ij}^2 + \gamma_{ij} (2\pi r_{ij}) \cos \alpha_{ij} \right\} + \left| k \frac{q_i . q_j}{r_{ij}^2} \right| \quad \right] \tag{10}$$

AAN is derived from the ratio of the volume-based median particle size to the average equivalent spherical volume derived from BET gas adsorption (Pickrell, 2007). Hence, AAN = $[(d_{50}.\ \rho_{He}.S_{BET}.g)/6\ ]^3$ in which SBET is mass specific surface area of the particle. When subjected to F_d, Higashitani *et al.* (2001) determined a power law that controls the relationship between the average number of particles in a broken agglomerate and F_d/F_{coh}. Using a modified discrete element method, Higashitani *et al.* (2001) approximated the average number of particles to be equal to $27.9 \times (F_d/F_{coh})^{-0.872}$. We summarize the above arguments as a conceptual model in Fig. 8.

Table 4. Simplified overview of compulsory input parameters for various EA models and powder characterization endpoints deemed necessary by OECD WPMN for complete hazard profiles of manufactured nanomaterials

Powder property	r	∅	ρ_{He}	d_p	PDI	RH	d_{50}	α	A
Considered as compulsory input parameter to EA models?	Yes (via powder bulk density)	No, but can be determined from data library (Lide, 2004)	Yes	Yes	Yes, via particle size distribution	Yes (particularly as moisture content)	Yes	Yes	No, but can be determined from data library (Bergström, 1997)
Agreed by OECD WPMN?	Yes (via powder pour density)	No, but can be determined from data library (Lide, 2004)	No	Yes	Yes, via particle size distribution	Yes	Yes	Yes (as other relevant information)	No, but can be determined from data library (Bergström, 1997)

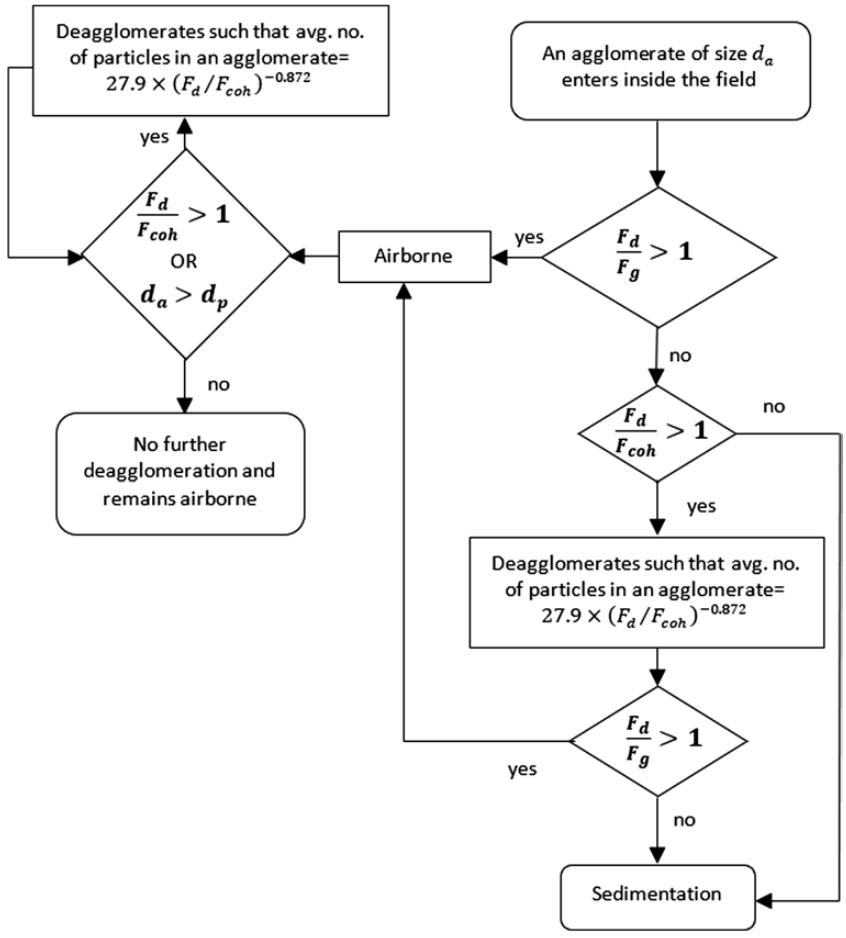

Figure 8. Schematic representation of the aerosolization criteria to satisfy for a falling down powder agglomerate.

Conclusions

The initial results from this study suggest that the dustiness of a powder can be attributed mainly to its eight characteristic physical properties (and two related to the process) for a continuous drop configuration. The compaction state and the ease to get electrostatically charged were the two most influencing properties of a powder for its tendency to emit airborne particles. When compared with each other, the former was observed to be 1.5 times (approx.) more influential than the latter. Although the former is the direct result of powder storage or packing conditions, the latter is dependent on the work function of the concerned metal element in the powder. The latter was also observed to be influenced by the moisture content of the powder as the tendency of powder particles to get electrostatically charged decreased by increasing the moisture content. This led the dustiness to positively correlate with low moisture content (<4% in the present case) and negatively correlate with relatively higher moisture content of the powder. The increase in the upward air stream velocity increased the drag force and reduced the mode size of the airborne particles. The tested hydrophobic powder was observed to generate relatively higher concentrations of nano- and sub-micro-sized airborne agglomerates than its hydrophilic counterpart which tended to generate more microparticles. Moreover, the effect of RH on reducing the powder dustiness was more pronounced for the hydrophilic powder than the hydrophobic one. We determined the two ratios, F_d/F_g and F_d/F_{coh}, to govern the concentration and mode size of the generated airborne particle agglomerates. These initial results, thus, can help to produce powders with low-emission potential, i.e. safe-by-design and eventually model dustiness to render powder handling operations safe-by-process.

Supplementary Data

Supplementary data are available at *Annals of Work Exposures and Health* online.

Acknowledgements

For the results presented in this study, the authors acknowledge the funding from EU H2020 caLIBRAte (grant agreement 686239), EU FP7 Marina (grant agreement 263215), and Nanodustiness projects as part of mandate M/461 'Nanotechnologies' as well as Dutch NanoNextNL project. We are also grateful to Marcel Moerman at TNO Utrecht to carry out the experiments and Dirk Dahman at IGF to contribute in the test protocol development for the study.

Declaration

The authors declare no conflict of interest relating to the material presented in this article. Its contents, including any opinions and/or conclusions expressed, are solely those of the authors.

References

Andreasen A, Hofman-Bang N, Rasmussen N. (1939) Uber das Staubungsvermogen der Stoffe [The dust-generating capacity of materials]. *Kolloidzeitschrift*; **86**: 70.

Bach S, Schmidt E. (2008) Determining the dustiness of powders – a comparison of three measuring devices. *Ann Occup Hyg*; **52**: 717–25.

Batsanov SS. (2001) Van der Waals radii of elements. *Inorg Mater*; **37**: 871–85.

Bergström L. (1997) Hamaker constants of inorganic materials. *Adv Colloid Interface Sci*; **70**: 125–69.

Bouillard J, Henry F, Marchal P. (2014) Rheology of powders and nanopowders through the use of a Couette four-bladed vane rheometer: flowability, cohesion energy, agglomerates and dustiness. *J Nanopart Res*; **16**: 2558–74.

Breum NO. (1999) The rotating drum dustiness tester: variability in dustiness in relation to sample mass, testing time, and surface adhesion. *Ann Occup Hyg*; **43**: 557–66.

Breum NO, Schneider T, Jørgensen O *et al.* (2003) Cellulosic building insulation versus mineral wool, fiberglass or perlite: installer's exposure by inhalation of fibers, dust, endotoxin and fire-retardant additives. *Ann Occup Hyg*; **47**: 653–69.

Brouwer DH, Links IH, De Vreede SA *et al.* (2006) Size selective dustiness and exposure; simulated workplace comparisons. *Ann Occup Hyg*; **50**: 445–52.

Brouwers HJH. (2006) Particle-size distribution and packing fraction of geometric random packings. *Phys Rev E*; **74**: 14.

Burdett G, Bard D, Kelly A *et al.* (2013) The effect of surface coatings on the dustiness of a calcium carbonate nanopowder. *J Nanopart Res*; **15**: 1311–27.

Butt HJ, Kappl M. (2010) *Surface and interfacial forces*. Weinheim, Germany: Wiley-VCH.

CEN EN 15051:3. (2013) *Workplace exposure – measurement of the dustiness of bulk materials – part 3: continuous drop method.*

Cheng W, Dunn PF, Brach RM. (2002) Surface roughness effects on microparticle adhesion. *J Adhes*; **78**: 929–65.

Cooper RG. (2008) The stage-gate idea-to-launch process-update: what's new and NexGen systems. *J Prod Innov Manag*; **25**: 213–32.

Dahmann D, Monz C. (2011) Determination of dustiness of nanostructured materials. *Gefahrstoffe Reinhaltung Luft*; **71**: 481–7.

Delgarm N, Sajadi B, Azarbad K *et al.* (2018) Sensitivity analysis of building energy performance: a simulation-based approach using OFAT and variance-based sensitivity analysis methods. *J Build Eng*; **15**: 181–93.

Dexter A, Tanner D. (1972) Packing densities of mixtures of spheres with log-normal size distributions. *Nat Phys Sci*; **238**: 31–2.

Ding Y, Stahlmecke B, Jiménez AS *et al.* (2015) Dustiness and deagglomeration testing: interlaboratory comparison of systems for nanoparticle powders. *Aerosol Sci Technol*; **49**: 1222–31.

Dörmann M, Schmid HJ. (2015) Simulation of capillary bridges between particles. *Procedia Eng*; **102**: 14–23.

Evans DE, Turkevich LA, Roettgers CT *et al.* (2013) Dustiness of fine and nanoscale powders. *Ann Occup Hyg*; **57**: 261–77.

Fransman W, Van Tongeren M, Cherrie JW *et al.* (2011) Advanced Reach Tool (ART): development of the mechanistic model. *Ann Occup Hyg*; **55**: 957–79.

Greason WD. (2000) Investigation of a test methodology for triboelectrification. *J Electrostat*; **49**: 245–56.

Hamby DM. (1994) A review of techniques for parameter sensitivity analysis of environmental models. *Environ Monit Assess*; **32**: 135–54.

Hamelmann F, Schmidt E. (2004) Methods for characterizing the dustiness estimation of powders. *Chem Eng Technol*; **27**: 844–7.

Harper W. (1951) The Volta effect as a cause of static electrification. *Proc R Soc Lond A*; **205**: 83–104.

Heitbrink WA, Todd WF, Cooper TC *et al.* (1990) The application of dustiness tests to the prediction of worker dust exposure. *Am Ind Hyg Assoc J*; **51**: 217–23.

Higashitani K, Iimura K, Sanda H. (2001) Simulation of deformation and breakup of large aggregates in flows of viscous fluids. *Chem Eng Sci*; **56**: 2927–38.

Hjemsted K, Schneider T. (1996) Documentation of a dustiness drum test. *Ann Occup Hyg*; **40**: 627–43.

Hughes D, Ogden TL. (1985) *BOHS technical guide no. 5, the selection and use of personal sampling pumps*. Leeds, UK: Science Reviews Ltd.

Ibaseta N, Biscans B. (2007) Ultrafine aerosol emission from the free fall of TiO_2 and SiO_2 nanopowders. *Kona Powder Part*; **25**: 190–204.

Jensen KA, Koponen IK, Clausen PA *et al.* (2009) Dustiness behaviour of loose and compacted Bentonite and organoclay powders: what is the difference in exposure risk? *J Nanopart Res*; **11**: 133–46.

Jensen K, Levin M. (2012) *NanoDevice D3.1a dustiness properties of powder ENPs*. Työterveyslaitos, Finland: EU NanoDevice Project.

Kulkarni P, Baron P, Willeke K. (2011) *Aerosol measurement: principles, techniques, and applications*. Hoboken, NJ: John Wiley & Sons, Inc.

Kurkela JA, Brown DP, Raula J *et al.* (2008) New apparatus for studying powder deagglomeration. *Powder Technol*; **180**: 164–71.

Levin M, Rojas E, Vanhala E *et al.* (2015) Influence of relative humidity and physical load during storage on dustiness of inorganic nanomaterials: implications for testing and risk assessment. *J Nanopart Res*; **17**: 1–13.

Lide D. (2004) *Handbook of chemistry and physics*. Boca Raton, FL: CRC Press.

Lidén G. (2006) Dustiness testing of materials handled at workplaces. *Ann Occup Hyg*; **50**: 437–9.

Marquart H, Heussen H, Le Feber M *et al.* (2008) 'Stoffenmanager', a web-based control banding tool using an exposure process model. *Ann Occup Hyg*; **52**: 429–41.

Matsusaka S, Masuda H. (2003) Electrostatics of particles. *Adv Powder Technol*; **14**: 143–66.

Mukherjee R, Gupta V, Naik S *et al.* (2016) Effects of particle size on the triboelectrification phenomenon in pharmaceutical excipients: experiments and multi-scale modeling. *Asian J Pharm Sci*; **11**: 603–17.

Nomura T, Satoh T, Masuda H. (2003) The environment humidity effect on the tribo-charge of powder. *Powder Technol*; **135–136**: 43–9.

O'Shaughnessy PT, Kang M, Ellickson D. (2012) A novel device for measuring respirable dustiness using low-mass powder samples. *J Occup Environ Hyg*; **9**: 129–39.

OECD. (2016) Physical-chemical properties of nanomaterials: evaluation of methods applied in the OECD-WPMN testing programme. Available at http://www.oecd.org/officialdocuments/publicdisplaydocumentpdf/?cote=ENV/JM/MONO(2016)7&doclanguage=en. Accessed 27 July 2018.

Pensis I, Mareels J, Dahmann D *et al.* (2010) Comparative evaluation of the dustiness of industrial minerals according to European standard EN 15051, 2006. *Ann Occup Hyg*; **54**: 204–16.

Pickrell J. (2007) Biomedical responses and toxicity of nanoparticles. In Gupta R, editor. *Veterinary toxicology: basic and clinical principals*. New York, NY: Academic Press. pp. 305–12.

Prescot J, Barnum R. (2000) Whitepaper on powder flowability. Pharmaceutical Technology. Available at https://www.powderbulk.com/enews/2014/whitepaper/jenike042014.pdf. Accessed 27 July 2018.

Rasmussen K, Mast J, De Temmerman P-J *et al.* (2014) Titanium dioxide, NM-100, NM-101, NM-102, NM-103, NM-104, NM-105: characterisation and physico-chemical properties. EU-JRC Policy Reports. Available at http://publications.jrc.ec.europa.eu/repository/bitstream/JRC86291/lbna26637enn.pdf. Accessed 27 July 2018.

Schneider T, Jensen KA. (2008) Combined single-drop and rotating drum dustiness test of fine to nanosize powders using a small drum. *Ann Occup Hyg*; **52**: 23–34.

Seipenbusch M, Rothenbacher S, Kirchhoff M *et al.* (2010) Interparticle forces in silica nanoparticle agglomerates. *J Nanopart Res*; **12**: 2037–44.

Shandilya N, Morgeneyer M, Le Bihan O. (2015) First development to model aerosol emission from solid surfaces subjected to mechanical stresses: II. Experiment-theory comparison, simulation and sensibility analysis. *J Aerosol Sci*; **89**: 1–17.

Tsai CJ, Huang CY, Chen SC *et al.* (2011) Exposure assessment of nano-sized and respirable particles at different workplaces. *J Nanopart Res*; **13**: 4161–72.

Tsai CJ, Wu CH, Leu ML *et al.* (2009) Dustiness test of nanopowders using a standard rotating drum with a modified sampling train. *J Nanopart Res*; **11**: 121–31.

van Ommen JR, Valverde JM, Pfeffer R. (2012) Fluidization of nanopowders: a review. *J Nanopart Res*; **14**: 737.

Yao J, Zhang Y, Wang C-H *et al.* (2004) Electrostatics of the granular flow in a pneumatic conveying system. *Ind Eng Chem Res*; **43**: 7181–99.

Zalk DM, Paik SY, Swuste P. (2009) Evaluating the control banding nanotool: a qualitative risk assessment method for controlling nanoparticle exposures. *J Nanopart Res*; **11**: 1685–704.